COMPARATIVE STUDIES OF LEVITATION AND CONTROL PERFORMANCES OF TWO TYPES OF SINGLE-AXIS CONTROLLED REPULSIVE TYPE MAGNETIC BEARING

S. C. Mukhopadhyay, T. Ohji, T. Kuwahara, M. Iwahara, S. Yamada and F. Matsumura
Laboratory of Magnetic Field Control and Applications,
Faculty of Engineering, Kanazawa University,
Kodatsuno 2-40-20 Kanazawa 920 Japan

SUMMARY

Single-axis controlled repulsive type magnetic bearings have the advantages of simplified control schemes and less numerous electromagnets. The bearing system employed can be one of two types of machine configurations: (1) Vertical-shaft machines, (2) Horizontal-shaft machines. Prototype models of each type have been developed and experiments conducted in our laboratory. This paper discusses different aspects such as design of bearing systems and configuration, levitation, control, vibration and disturbance attenuation characteristics etc. of two types of schemes of repulsive type magnetic bearings. The controllers of both systems have been configured around digital signal processors.

INTRODUCTION

In recent times, magnetic bearings offering numerous advantages such as long life, extreme reliability, frictionless nature, lubrication free operation, low losses, adjustable damping and stiffness characteristics are becoming indispensable in applications such as turbomolecular pumps, space applications, vacuum and clean room atmosphere, fly-wheel energy storage systems and so on. Because in the presence of active control in active magnetic bearings (AMB) the stiffness and damping characteristics can be adjusted according to requirements along the controlled axis, AMBs are more commonly used in critical industrial applications but incur more cost, need complicated controllers and lots of electromagnets. Repulsive type magnetic bearings consisting of permanent magnets and controlled electromagnets have the advantages of a lower number of electromagnets and simplified control schemes compared to active magnetic bearings. Many research papers have been published on magnetic bearings using permanent magnets (PM) [1-4]. But the satisfactory operation of this type of

magnetic bearing system is strongly dependent on the characteristic of the permanent magnet and its configuration in the bearing system. The permanent magnet configuration is very important because it determines the characteristics along the passive axis. The bearing system employed can be one of two types of machine configurations - (1) Vertical-shaft machines and (2) Horizontal-shaft machines. In type (1) the levitation force and stiffness characteristics are decoupled from each other resulting in simpler magnet configurations. In type (2) the levitation force and stiffness characteristics are coupled to each other and there must be a trade-off between the two to obtain an optimum characteristic. Prototype models of each type have been developed and experiments conducted in our laboratory. This paper discusses the different aspects such as design of bearing systems and configuration, levitation, control, vibration and disturbance attenuation characteristics etc. of two types of schemes of repulsive type magnetic bearings. The controllers of both the systems have been configured around digital signal processors.

CONFIGURATION OF BEARING SYSTEM FOR VERTICAL-SHAFT MACHINE

The system configuration developed in our laboratory is shown in Fig. 1 and the corresponding PM configuration is shown in Fig. 2. Both that stator and rotor permanent magnet are made of strontium-ferrite magnet. One gap sensor is used to detect the position of the rotor along the vertical direction, one electromagnet is used for rotor positioning, and the control is provided along the vertical axis. Improvement of either levitation force or radial stiffness can be done without sacrificing the other. The active control axis is the same as the levitation direction in this scheme. The principal data are: length of rotor = 420mm, mass of rotor = 5.5kg, diameter of rotor = 200mm.

CONFIGURATION OF BEARING SYSTEM FOR HORIZONTAL-SHAFT MACHINE

The system developed in the laboratory is shown in Fig. 3. The rotor is levitated due to the repulsive force acting between the stator and rotor permanent magnets along the vertical-axis. The unstable system is stabilized by active control along the horizontal axis. No active control has been provided along the vertical axis. Since the rotor is levitated due to the repulsive force, the symmetrical PM configuration described earlier cannot be used in this configuration. In order to achieve better disturbance attenuation characteristics, higher stiffness is desirable, which has been achieved by an optimum configuration of permanent magnets. The configuration of permanent magnets for this type

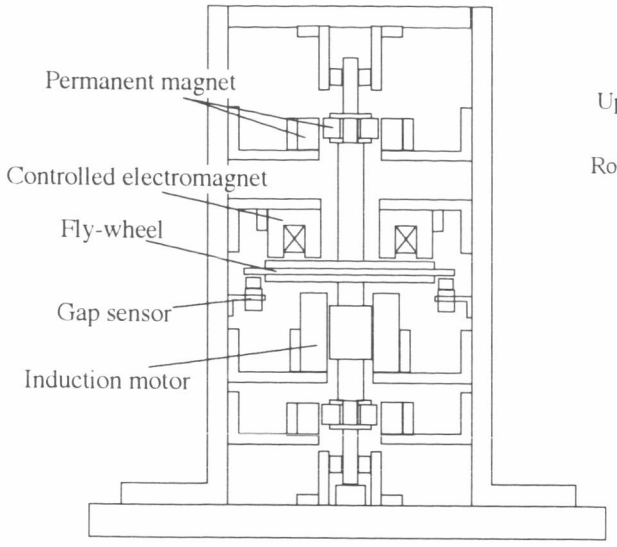

Figure 1. Bearing system configuration.
(Vertical-shaft machine)

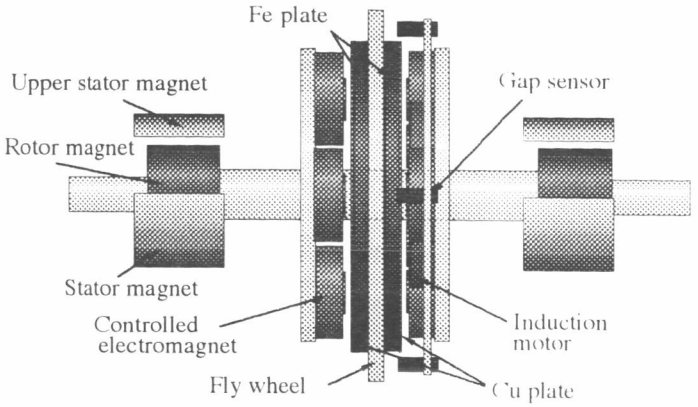

Figure 3. Bearing system configuration.
(Horizontal-shaft machine)

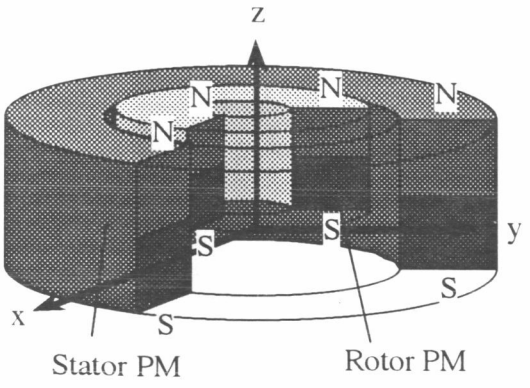

Figure 2. PM configuration.
(Vertical-shaft machine)

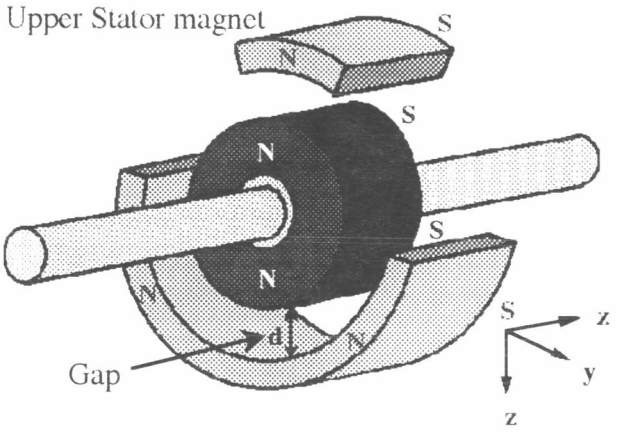

Figure 4. PM configuration
(Horizontal-shaft machine)

of magnetic bearing system is shown in Fig. 4. The stator permanent magnet is made of Neodymium-iron-boron (Nd-Fe-B) material and the rotor is of Strontium-ferrite material. The motor used in this study is a normal induction motor. Four electromagnets are used for the axial control but they are not separately controlled, all are connected in series. A gap sensor is used to sense rotor position and is of eddy-current type giving an output of 1V/mm. The principal data are: length of rotor = 510mm, mass of rotor = 8kg, diameter of rotor = 220mm.

LEVITATION AND STIFFNESS CHARACTERISTICS

In permanent magnet bearing systems, it is very important to know the force and stiffness characteristics operating between the stator and rotor permanent magnets. We have analyzed the above

characteristics with the help of the finite element method. Since attenuation of disturbance along the uncontrolled passive radial direction is very important for the stability of the system, higher stiffness is desirable.

With the help of three-dimensional finite element analysis, the repulsive force and stiffness characteristics are calculated for the vertical-shaft machine. The force as well as stiffness depend on the material characteristic and the configuration of PMs in the system. We have calculated the repulsive forces for two types of PM materials. If only the rotor material is replaced by Nd-Fe-B magnet, the improvement is not significant but if both stator and rotor PM is replaced by Nd-Fe-B magnet, a great improvement of the characteristics are observed. Fig. 5 shows the relative characteristics along the vertical axis and Fig. 6 is that for the horizontal axis. Since control is provided along the vertical axis, the passive stiffness along that axis is not so important. Fig. 7 shows the stiffness characteristic along the radial direction.

Another method by which the repulsive force and stiffness characteristics can be improved is by providing a small gap between the permanent magnets of the stator PM assembly or rotor PM assembly. Fig. 8 shows the characteristic where a gap of 1mm has been provided in the rotor PM assembly and the stator is kept as it is. It is seen that there is a slight improvement in repulsive force.

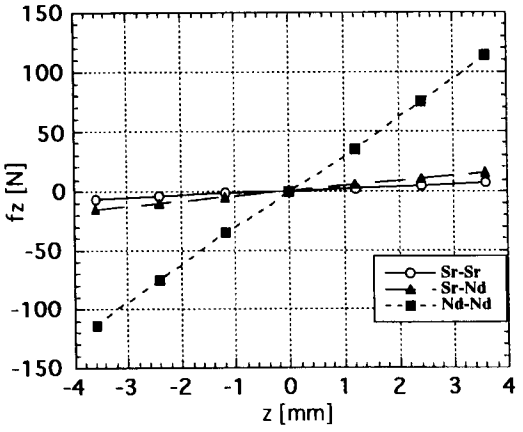

Figure 5. Repulsive force characteristic for different material along vertical-direction.

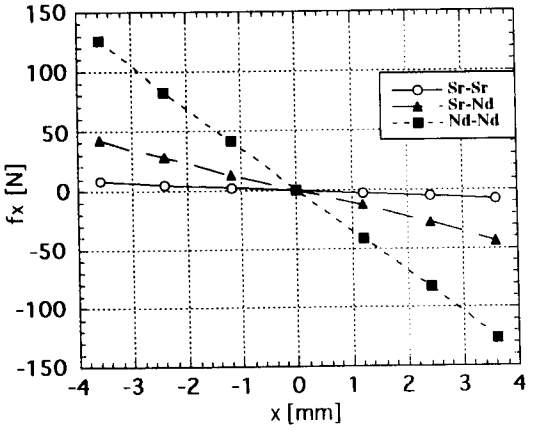

Figure 6. Repulsive force characteristic for different material along radial-direction.

Instead of configuring the Pms as NSNS.., if it is configured as NSSN..and is provided with a small gap between two successive magnets, both the stiffness and the levitation force are improved. This has been described in detail in [5]. This configuration needs a complicated arrangement for holding the magnets in their respective positions.

Since the vertical-shaft configuration is a well established one, we will not go into great detail. We have developed a simple laboratory model using low cost strontium-ferrite magnets with NSNS configuration. The experimental characteristics are measured and are shown in Fig. 9 and 10 respectively.

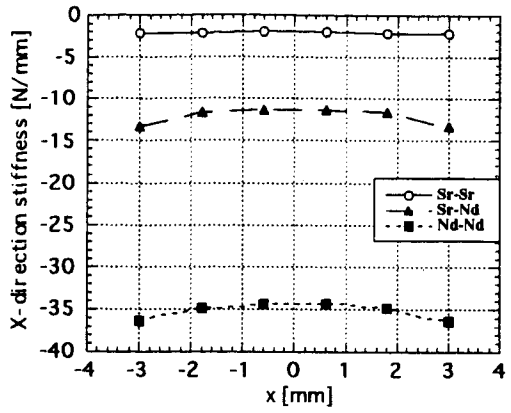

Figure 7. Stiffness characteristic for different material along radial-direction.

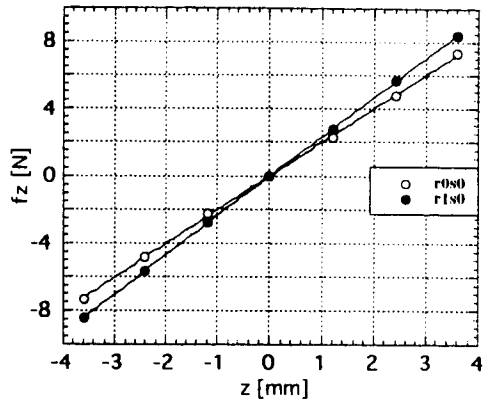

Figure 8. Repulsive force characteristic having gap in PM assembly.

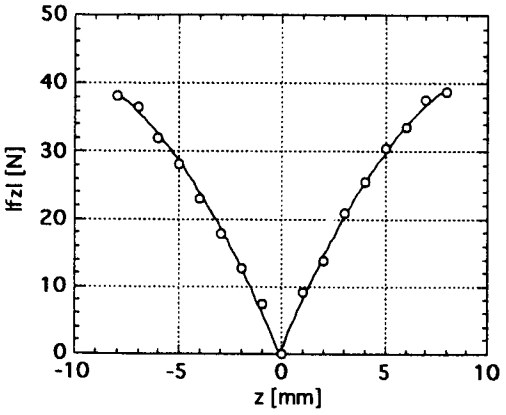

Figure 9. Experimental levitation force for system #1.

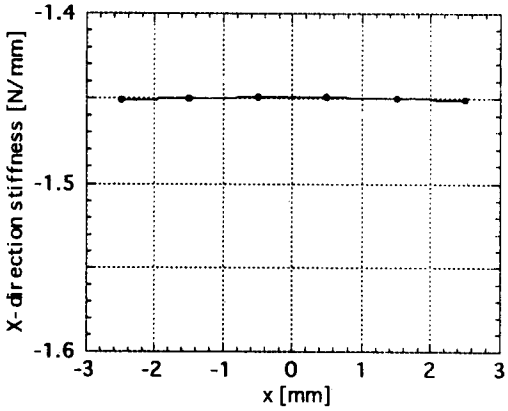

Figure 10. Experimental stiffness characteristic for system #1.

For the horizontal-shaft configuration, the symmetrical PM configuration as discussed earlier will be of no use as it results in zero levitation force along the vertical axis. In order to achieve better radial stiffness, a section of PM is placed on the upper half of the stator. Fig. 11 shows the 2-dimensional view of the PM configuration. Placement of the upper stator permanent magnet will reduce the levitation force, so the arc length θ should be selected critically. With the help of FE analysis a trade-off has been achieved. The PM configuration shown in Fig. 4 is an open boundary problem and is not an axi-symmetric one if three-dimensional view is taken. Using three-dimensional finite element analysis, more precise results can be obtained at the cost of a large computer memory requirement and long computation time. Considering the movement of the rotor with respect to the stator configuration, the model can be reduced to a two-dimensional one for the analysis to be made more practical, yet obtaining relatively precise results. Also, the complexity of three-dimensional analysis can be avoided. The sectional view of Fig. 4 has been shown in Fig. 12 for two-dimensional finite element analysis. Different two-dimensional views are obtained when the bearing system is cut at different angles; the

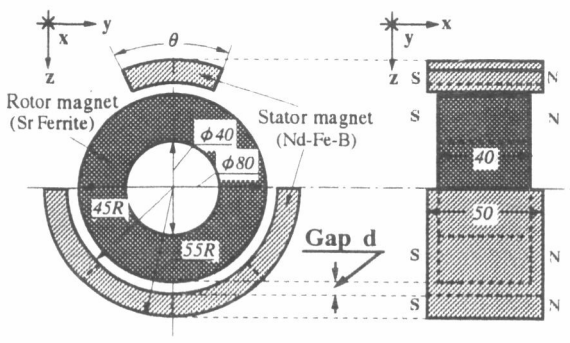

Figure 11. 2-D of PM configuration of system #2.

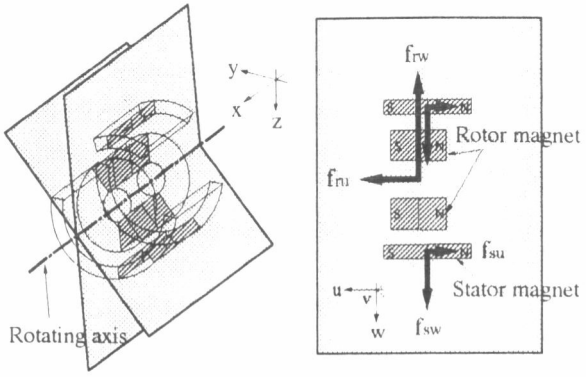

Figure 12. Sectional view of PM configuration.

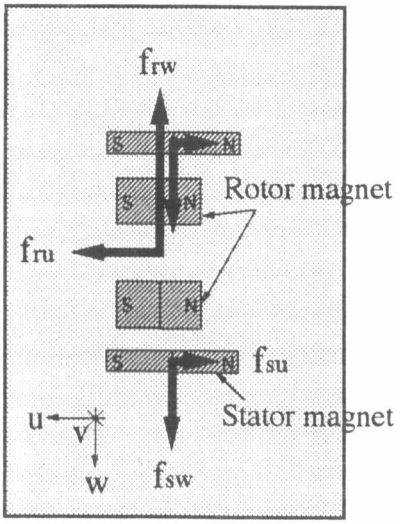

(a) 2-D view of section near 90° cutting angle.

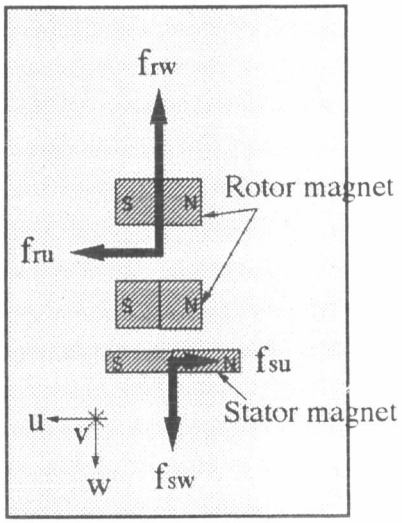

(b) 2-D view of section near 0° cutting angle.

Figure 13. 2-D view of the model.

cutting plane makes with the horizontal plane passing through the rotating axis.

Fig. 13a shows the view when the cutting plane makes an angle of nearly 90° with the horizontal plane and Fig. 13b shows the view when the cutting plane makes nearly 0° with the horizontal plane. We have taken 19 such views of each rotor position with respect to the stator at 10° intervals along the rotor surface. For the field analysis MSC markets the software package

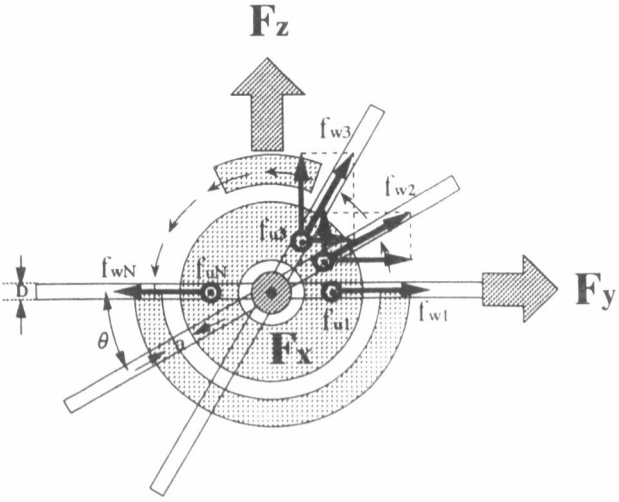

Figure 14. Forces on rotor section.

EMAS, which has been used and the repulsive forces f_{ru}, f_{su}, f_{rw} and f_{sw} as shown in Fig. 12 are calculated from the field solution. Resultant forces along u and w are given by

$$f_u = |f_{ru} - f_{su}| \quad \text{------(1)} \qquad f_w = |f_{rw} - f_{sw}| \quad \text{------(2)}$$

Fig. 14 shows all the forces acting on different sections of the model. By adding the forces vectorially the resultant forces along the three axes x, y and z are given by

$$F_x = f_{u1} + f_{u2} + ... + f_{uN} \quad \text{------(3)}$$

$$F_y = f_{w1}\cos\theta_1 + f_{w2}\cos\theta_2 + ... + f_{wN}\cos\theta_N \quad \text{----(4)}$$

$$F_z = f_{w1}\sin\theta_1 + f_{w2}\sin\theta_2 + ... + f_{wN}\sin\theta_N \quad \text{----(5)}$$

This method of calculation forms a two-dimensional database which helps to understand easily the variation of repulsive forces with rotor movement. In order to find the optimum PM configuration by changing the upper PM section, we have calculated the forces and stiffness characteristics along the vertical i.e., the z-direction.

By changing the arc section θ we have calculated the force and stiffness characteristics. Fig. 15a and b shows the variation of repulsive force and stiffness characteristics with the gap distance for different values of θ. It is seen that higher stiffness is achieved at the cost of repulsive force. Since higher repulsive force is necessary from the levitation point of view, a trade-off between the two is achieved and $\theta = 45°$ is chosen for our laboratory model.

The levitation and stiffness have also been analyzed by the three-dimensional finite element method and also measured experimentally. Fig. 16a and b shows the levitation and stiffness characteristics by 2-D, 3-D and experimental methods for the laboratory model.

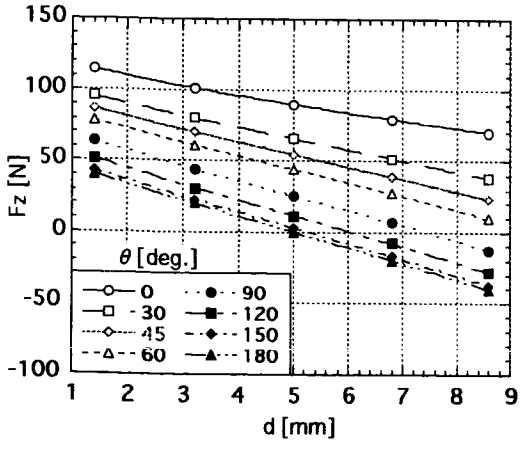

Figure 15(a). Variation of repulsive force with gap-distance for different sections.

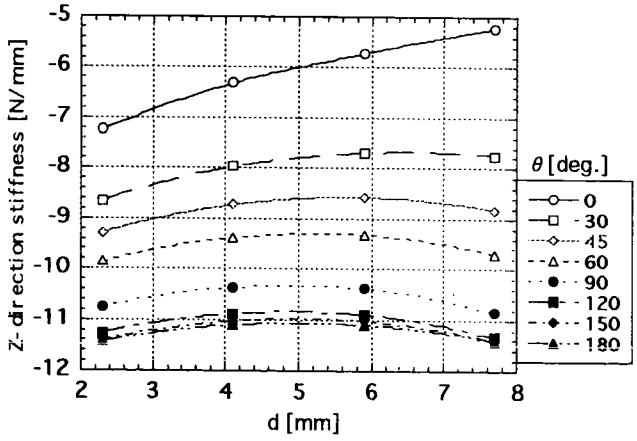

Figure 15(b). Stiffness characteristic for different sections.

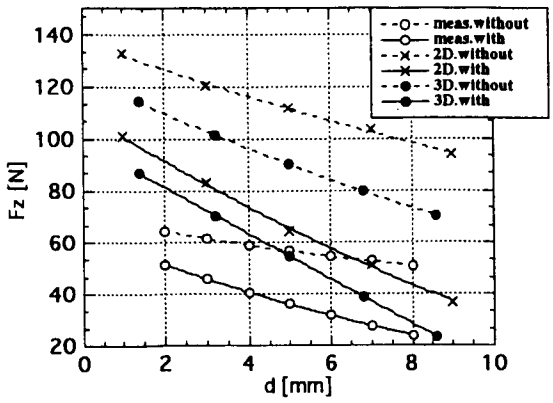

Figure 16(a). Comparative values of repulsive forces.

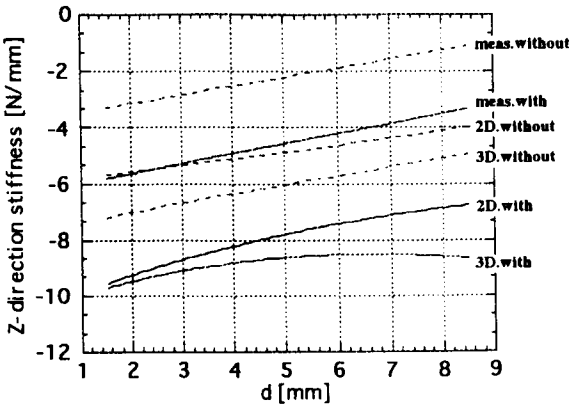

Figure 16(b). Comparative stiffness characteristics.

SYSTEM MODELING

Both the systems are expressed in the form of state-space models. The modeling of repulsive type magnetic bearings have been described in detail in [6]. In this section, simplified models of two systems have been considered. For this purpose, the operating forces are expressed analytically.

The repulsive force characteristic along the controlled axis can be expressed as

$$f_{PM,i} = S_i \cdot x + F_{0,i} \qquad \text{-------(6)}$$

where I=1 for system #1 (Vertical-shaft machine) and I=2 for system #2 (Horizontal-shaft machine). S_i is the slope of characteristic of system #2 and is expressed as N/m. $F_{o,i}$ is the force at the nominal operating point for system #1, in N. x is the displacement from the nominal operating point.

The electromagnet quantities are expressed by

$$e_i = L_i \frac{di_i}{dt} + R_i i_i \qquad \text{-----(7)}$$

$$f_i = k\left(\frac{i_i}{g_i}\right)^2 \qquad \text{-----(8)}$$

where L_i and R_i are the inductance and resistance of the electromagnet of system #1. k is a constant which depends on the structure of the magnet and the number of turns.

Assuming all the four electromagnets used for system #2 are identical, the total operating forces will be four times that given by eqn (8).

Linearizing the operating characteristic of the electromagnet around the normal equilibrium operating point and expressing by the deviated quantities from the steady state values, we get

$$e_i' = L_i \frac{di_i'}{dt} + R_i i_i' \qquad \text{----(9)}$$

$$f_i' = 2F_{e,i}\left(\frac{i_i'}{I_{0,i}} - \frac{g_i'}{W}\right) \qquad \text{----(10)}$$

where Fe, Io and W are the force, current and gap-distance at the nominal operating point. At steady-state, the following relationships hold good.

$$For\ system\ \#\ 1, \quad F_{e1} + 2F_{01} - m_1 g = 0 \quad -----(11)$$

$$For\ system\ \#\ 2, \quad 4F_{e2} - 2F_{02} = 0 \quad -----(12)$$

The dynamic equation of motion is given by,

$$For\ system\ \#\ 1, \quad m_1 \frac{d^2 x_1}{dt^2} = f_{e1} + 2f_{01} - m_1 g \quad ----(13)$$

$$For\ system\ \#\ 2, \quad m_2 \frac{d^2 x_2}{dt^2} = 4f_{e2} + 2f_{02} \quad -----(14)$$

All the variable parameters are linearized around the nominal operating point. Taking the gap-deviation from the nominal point, its derivative and the current deviation from the nominal point, the state-space model is given by,

$$\frac{d}{dt}\begin{bmatrix} x' \\ \dot{x}' \\ i' \end{bmatrix} = \begin{bmatrix} 0 & 1 & 0 \\ \frac{2S}{m} + \frac{2}{mW}\sum_i F_i & 0 & \frac{2}{mI}\sum_i F_i \\ 0 & 0 & -\frac{r}{L} \end{bmatrix} \begin{bmatrix} x' \\ \dot{x}' \\ i' \end{bmatrix} + \begin{bmatrix} 0 \\ 0 \\ \frac{1}{L} \end{bmatrix} e' \quad ----(15)$$

$$y = \begin{bmatrix} 1 & 0 & 0 \end{bmatrix} \begin{bmatrix} x' \\ \dot{x}' \\ i' \end{bmatrix} \quad ----(16)$$

The parameters used in the model are explained below.

x'	: Gap derivation from nominal state
i'	: Current derivation of electromagnet from nominal state
e'	: Incremental input voltage to electromagnet
m	: Mass of rotor
F_i	: Attractive force at steady state
I	: Nominal current
W	: Nominal gap
r	: Resistance of electromagnet
L	: Inductance of electromagnet
R,S	: Constant used in permanent magnet equation

The performance of the system represented by the state-space model in eqns. (15) and (16) has been simulated with the help of MATLAB. The block diagram representation of the model for the performance simulation is shown in Fig. 17. The values of different parameters used in the model are listed in Table 1. Using the values of the parameters, the A and B matrices are given by,
for system #1,

$$A_1 = \begin{bmatrix} 0 & 1 & 0 \\ 7547.9 & 0 & 12.03 \\ 0 & 0 & -68.05 \end{bmatrix} \quad B_1 = \begin{bmatrix} 0 \\ 0 \\ 27.78 \end{bmatrix} \quad ----(17)$$

for system #2,

$$A_2 = \begin{bmatrix} 0 & 1 & 0 \\ 5585 & 0 & 2.654 \\ 0 & 0 & -60.5 \end{bmatrix} \quad B_2 = \begin{bmatrix} 0 \\ 0 \\ 5.165 \end{bmatrix} \quad ----(18)$$

Fig. 18 shows the simulated response characteristics of system #1 and Fig. 19 is that for system #2.

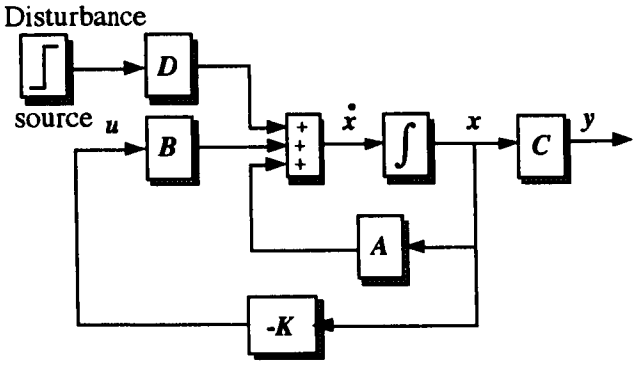

Figure 17. Simulation block diagram.

Table 1. Main parameters of systems.

PARAMETER	SYSTEM#1	SYSTEM#2
m	5.5kg	8kg
S	0.49×10^{4} N/m	1.18×10^{4} N/m
F_0	15.97 N	11.76 N
F_e	21.46 N	5.88 N
L	0.036 H	0.194 H
R	2.45 Ohm	11.72 Ohm
I_0	0.48 A	1.0 A
W	0.001 m	0.002 m

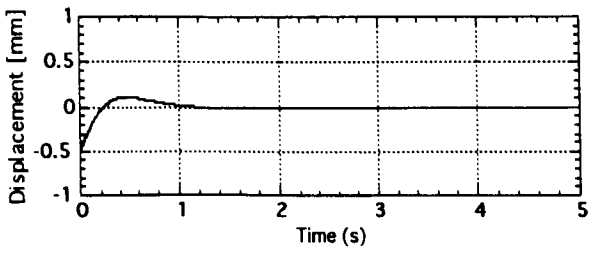

Figure 18. Simulated response of system #1.

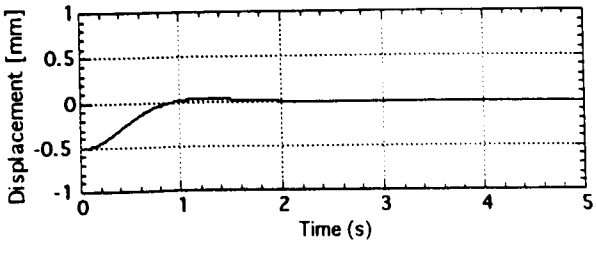

Figure 19. Simulated response of system #2.

Using eqns (15) and (16) for the stability of the system which is unstable in nature, an optimum integral type servo control system has been constructed. Using the Matlab control system toolbox, the Riccati equation is solved to obtain the feedback coefficients. The experiments are carried out by configuring the controller around the digital signal processor. The block diagram representation of the control system is shown in Fig. 20. The inputs to the controller are the gap-deviation, its derivative and the current deviation of the electromagnet. The output is the control signal to the power amplifier. The DAC output is represented as

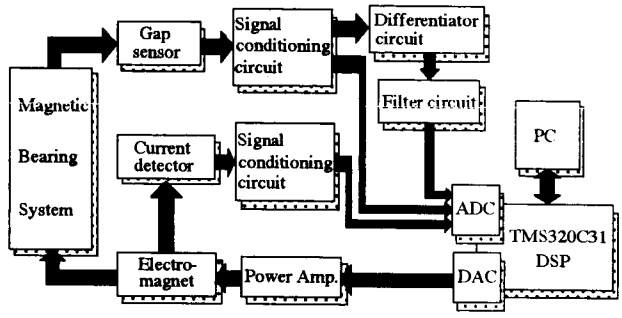

Figure 20. Controller block diagram representation.

$$e' = -\left(k_1 x' + k_2 \frac{dx'}{dt} + k_3 i' + \int x'\, dt\right) \quad -----(19)$$

With the help of the controller, the rotors are stabilized. Fig. 21 shows the vibration characteristic along the control axis of the vertical-shaft machine. Fig. 22 shows that of horizontal-shaft machine. It is seen that the level of vibration is similar. This is due to the fact that the same type of controller has been employed for the axial stabilization.

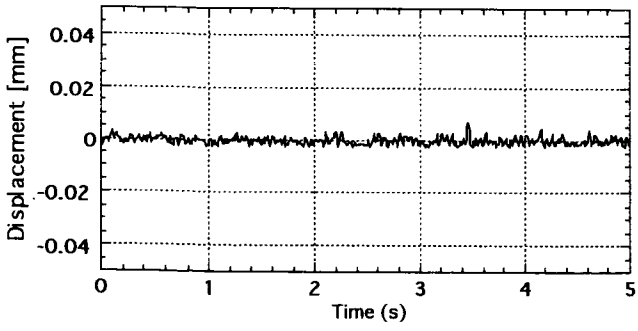

Figure 21. Vibration characteristic of system #1.

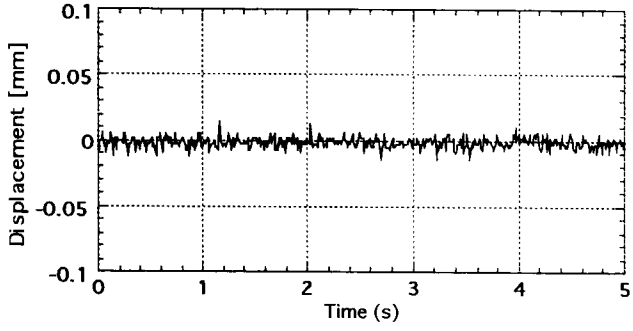

Figure 22. Vibration characteristic of system #2.

The important thing to be considered is the disturbance attenuation characteristic along the passive control axis of the two systems. Since the PM configuration for system #1 is symmetrical, disturbances along the passive radial direction will be damped out to zero with time. The higher the stiffness, the faster the stabilization. But in system #2, the presence of an upper stator magnet has a strong influence [7]. When disturbances are created, the system shows overshoot and returns back

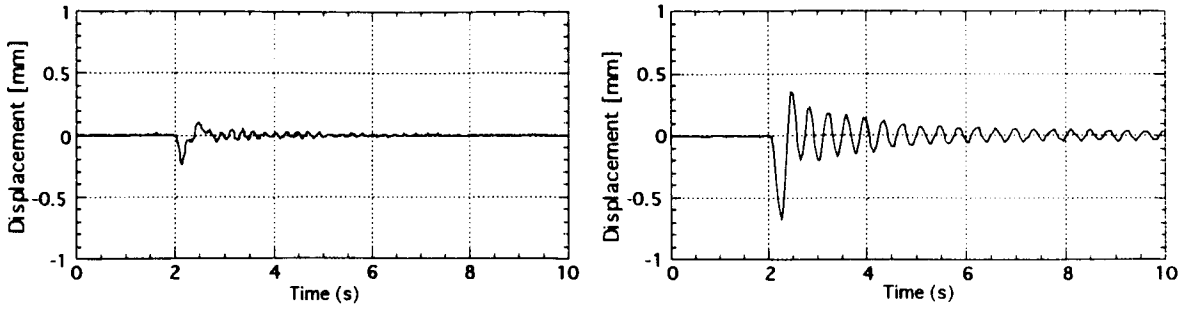

(a) With upper stator magnet. (b) Without upper stator magnet.

Figure 23. Disturbance characteristic at zero speed.

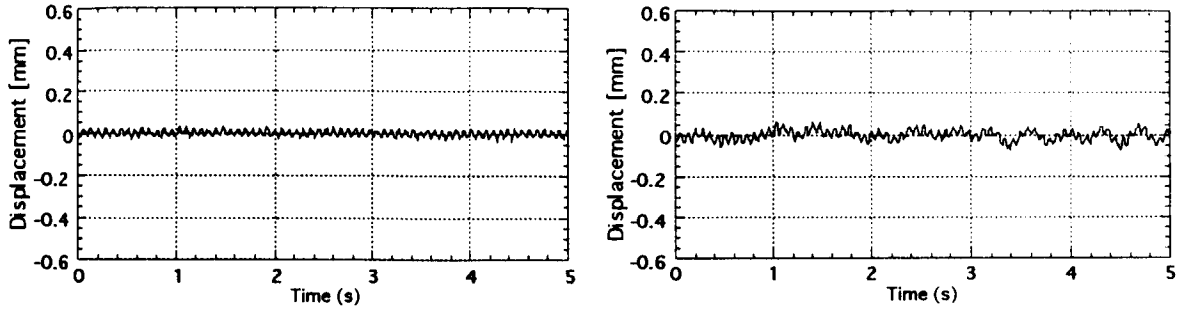

(a) With upper stator magnet. (b) Without upper stator magnet.

Figure 24. Vibration characteristic at 800rpm.

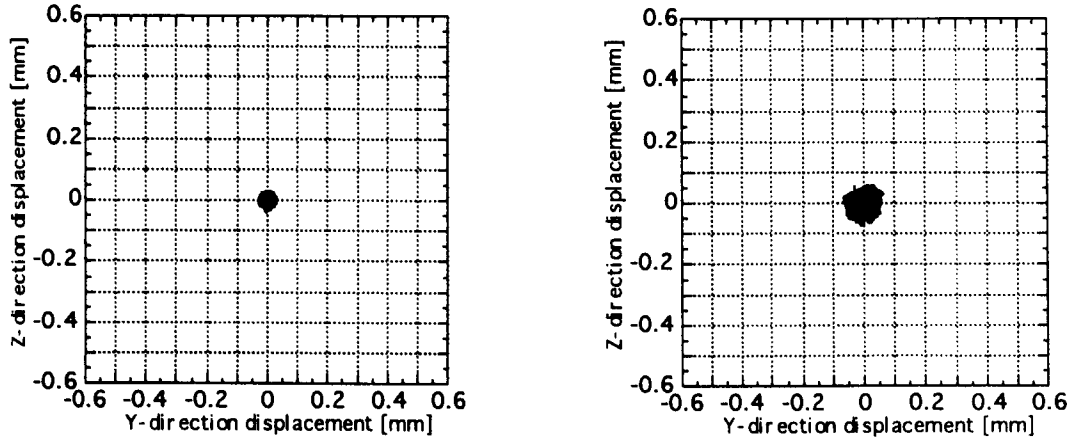

(a) With upper stator magnet. (b) Without upper stator magnet.

Figure 25. z-axis vibration vs. y-axis vibration at 800rpm.

to the original state after some time. Fig. 23a and b shows the disturbance characteristics at zero speed with and without the upper stator magnet respectively. It is seen from Fig. 23 that for the same magnitude of disturbing force the effect is almost one-third in the case with an upper stator magnet system compared to that without an upper stator magnet system. In order to verify the response characteristic while the rotor is in motion, the motor is driven at low speed. Due to the presence of harmonic torques, there is a lot of disturbing force during low speed operation of the motor. Fig. 24a and b shows vibration characteristics at 800rpm with and without the upper stator magnet. Fig. 25a

and b shows the y-axis vibration vs. z-axis vibration characteristics at 800rpm. It is seen that the vibration level is less for the system with the upper stator magnet.

CONCLUSION

In this paper, we have discussed two types of single-axis controlled repulsive type magnetic bearing systems. Their configuration, permanent magnet arrangement, levitation, stiffness characteristics and control performances have been described. For the horizontal-shaft machine, an optimum permanent magnet configuration has been obtained which reduces the levitation force but improves the radial stiffness characteristic. The choice of the system type depends on the application and system requirements.

REFERENCES

1. J. P. Yonnet, "Passive Magnetic Bearing with Permanent Magnets," *IEEE Trans. on Magnetics,* Vol-MAG 14, No. 5, pp. 803-805, Sept. 1978.
2. J. P. Yonnet, "Passive Magnetic Bearing and Couplings," *IEEE Trans. on Magnetics,* Vol-MAG 17, No. 1, pp. 1169-1173, Sept. 1981.
3. J. P. Yonnet, S. Hemmerlin, E. Rulliere and G. L. Emarquand, " Analytical Calculation of Permanent Magnet Couplings," *IEEE Trans, on Magnetics,* Vol-MAG 29, No. 6, pp. 2932-2934, Nov. 1993.
4. J. Delamare, E. Rulliere and J. P. Yonnet, "Classification and Synthesis of Permanent Magnet Bearing Configuration," *IEEE Trans. on Magnetics,* Vol-MAG 31, No. 6, pp. 4190-4192, Nov. 1995.
5. J. P. Yonnet, "Analytical Calculation of Magnetic Bearings," *Proc. of Fifth International Workshop on Rare Earth-Cobalt Permanent Magnets and their Applications,* June 7-10, 1981, pp. 199-216, Virginia, USA.
6. S. C. Mukhopadhyay, T. Ohji, M. Iwahara, S. Yamada and F. Matsumura, "A New Repulsion Type Magnetic Bearing," *Proc. of IEEE PEDS,* Vol. 1, pp. 12-18, Singapore, May 26-29, 1997.
7. S. C. Mukhopadhyay, T. Ohji, S. Yamada and F. Matsumura, "Disturbance Attenuation and Faster Stabilization via Permanent Magnet Placement on Repulsion Type Magnetic Bearing," *Proc. of IEEE PEDS,* Vol. 1, pp. 255-261, Singapore, May 26-29, 1997.